ELSEVIER Journal of Computational and Applied Mathematics 103 (1999) 33–41

JOURNAL OF COMPUTATIONAL AND APPLIED MATHEMATICS

Three dimensional supersonic flow analysis over a satellite vehicle launcher

A.L. De Bortoli

Federal University of Rio Grande do Sul, Department of Pure and Applied Mathematics, 90501-900, Porto Alegre (RS), Brazil

Received 3 February 1998

Abstract

The ever-widening applications of numerical calculations leads to a variety of new numerical methods, which are different in their solution algorithms as well as in the discretization of the governing equations. Despite this development, much work still remains in their improvement towards a fast, accurate and stable convergence. This work shows a numerical method for the solution of compressible and almost incompressible fluid flows using a finite volume, explicit Runge-Kutta multistage scheme, with central spatial discretization in combination with multigrid and preconditioning. Numerical tests are carried out for a vehicle launcher for Mach-number 3.75 and 2.0 using the Euler equations. © 1999 Elsevier Science B.V. All rights reserved.

Keywords: Supersonic flow; Satellite launcher; Numerical fluid flow; Finite volume; Multigrid

1. Introduction

The rapid evolution of computational fluid dynamics has been driven by the need of faster and more accurate methods for the calculation of flow fields around configurations of technical interest. With the advent of more powerful computers and more efficient algorithms the researchers have in recent years computed more detailed and sophisticated simulations of fluid flow phenomena.

Numerical flow simulations have found their way into the aerodynamical design cycles of aerospace vehicles. Not only do these simulations reduce turn-around time and cost, but they also offer flow parameter variations which are not possible with wind tunnel testing. Even then, flows over aerodynamical configurations display flow phenomena with very different scales and with highly nonlinear behaviour.

The design of an aircraft or a launch vehicle involves the calculation of the flow behaviour during a full flight passing through various flow regimes. For transonic and supersonic flows, for example, sharp changes in the aerodynamical coefficients are observed due to instabilities presented in the flow. These instabilities are originated not only by strong viscous interactions in the boundary layer,

PII: S0377-0427(98)00238-6

but also by interactions between the shock wave and boundary layer. This indicates that a model employing the potential flow equations can not be used and one has to employ the Euler/Navier–Stokes equations.

Common methods used for the solution of fluid flows are based on finite differences, finite volumes, finite elements and boundary elements discretizations. Each of these methods has its advantages and disadvantages. Nevertheless, all these methods used for the simulation of fluid flows have the common feature that the domain has to be divided into a number of small cells of appropriate shape. The solution of the global system of governing equations delivers the variables at the mesh points.

The standard compressible method is employed in this work and consists of the use of the momentum equations to obtain the velocity components, the energy equation for the calculation of energy, the mass conservation equation for the computation of density and the state equation to obtain the pressure. The solver employs structured boundary fitted meshes with trapezoidal cell shapes.

For all the computations, the Euler/Navier–Stokes equations are solved using the finite volume explicit Runge–Kutta multistage scheme, which can be easily combined with multigrid and preconditioning. Attention is focused on the two major parts of the numerical algorithm. These are the spatial discretization and the time-stepping algorithm. With the spatial discretization of the governing equations we seek to obtain accurate solutions with as few as possible discrete points in the flow domain. Care must be taken to resolve the relevant flow phenomena, i.e., smoothly varying regions of inviscid flows, flow discontinuities as shocks and slip lines. Moreover, numerical analysis and well-known experience show that the choice of the spatial discretization also influences the convergence of the overall method to the desired steady-state flow regime.

Numerical tests are carried out for a launch vehicle for Mach-numbers 3.75 and 2.0 using the Euler equations. Results obtained for Mach 3.75 are compared with available experimental data.

2. Governing equations

The governing equations for nonviscous flows are the Euler equations. The three dimensional Euler equations for unsteady compressible inviscid flows in differential form reads [6]

$$\frac{\partial \boldsymbol{W}}{\partial t} + \frac{\partial \boldsymbol{F}_1}{\partial x} + \frac{\partial \boldsymbol{F}_2}{\partial y} + \frac{\partial \boldsymbol{F}_3}{\partial z} = 0, \tag{1}$$

where

$$\boldsymbol{W} = \begin{pmatrix} \rho \\ \rho u \\ \rho v \\ \rho w \\ \rho e \end{pmatrix}, \qquad \overline{F} = \begin{pmatrix} \rho u \boldsymbol{q} \\ \rho u \boldsymbol{q} + p\boldsymbol{i} \\ \rho v \boldsymbol{q} + p\boldsymbol{j} \\ \rho w \boldsymbol{q} + p\boldsymbol{k} \\ \rho H \boldsymbol{q} \end{pmatrix}, \qquad \overline{F} = \boldsymbol{F}_1\boldsymbol{i} + \boldsymbol{F}_2\boldsymbol{j} + \boldsymbol{F}_3\boldsymbol{k}, \tag{2}$$

and $\boldsymbol{F}_1$, $\boldsymbol{F}_2$ and $\boldsymbol{F}_3$ are the cartesian flux vector components. The total energy and total enthalpy are

$$E = e + \tfrac{1}{2}(u^2 + v^2 + w^2), \tag{3}$$

$$H = E + \frac{p}{\rho}, \tag{4}$$

where $\boldsymbol{q}$ is the velocity vector and e the internal energy. To close this system of equations, the state equation for a perfect gas is employed [7]

$$p = \rho RT = (\gamma - 1)\rho[E - \tfrac{1}{2}(u^2 + v^2 + w^2)], \tag{5}$$

where R is the gas constant, γ the specific heat ratio, ρ the fluid density, u, v and w are the velocity components, p is the pressure and T the temperature. Eq. (1) can be cast into the integral form [6]

$$\int_V \frac{\partial \boldsymbol{W}}{\partial t}\,\mathrm{d}V + \int_S (\bar{F}.\boldsymbol{n})\,\mathrm{d}S = 0, \tag{6}$$

where V and S represent the domain volume and its surface, respectively, and $\boldsymbol{n}$ is the normal vector to the surface.

3. Description of the numerical method

One of the differences among the various finite volume formulations known in the literature is the arrangement of the control volume for the flow variables [7]. The most frequently used schemes are the cell-centered, cell-vertex and node-centered approachs. Each of these schemes has its advantages and disadvantages. The discretization employed in this work is based on the cell-centered [4], and node-centered arrangements [7], as shown in Fig. 1. As Eq. (1) is valid for an arbitrary control volume, it is also valid for $V_{i,j,k}$, which means

$$\frac{\partial \boldsymbol{W}_{i,j,k}}{\partial t} = -\frac{1}{V_{i,j,k}} \int_S (\bar{F}.\boldsymbol{n})\,\mathrm{d}S. \tag{7}$$

The finite volume discretization based on the central averaging is not dissipative [6]. The numerical procedure does not converge to the steady state solution when the high frequency oscillations of error in the solution are not damped. The dissipation vector $\boldsymbol{D}_{i,j,k}$ is introduced by adding dissipative fluxes as follows [5]:

$$\frac{\partial \boldsymbol{W}_{i,j,k}}{\partial t} = -\frac{1}{V_{i,j,k}}[\boldsymbol{Q}_{i,j,k} - \boldsymbol{D}_{i,j,k}]. \tag{8}$$

The dissipation operator is a blend of second and fourth order differences, and is defined according to [9]

$$\boldsymbol{D}_{i,j,k} = d_{i+1/2,j,k} - d_{i-1/2,j,k} + d_{i,j+1/2,k} - d_{i,j-1/2,k} + d_{i,j,k+1/2} - d_{i,j,k-1/2}, \tag{9}$$

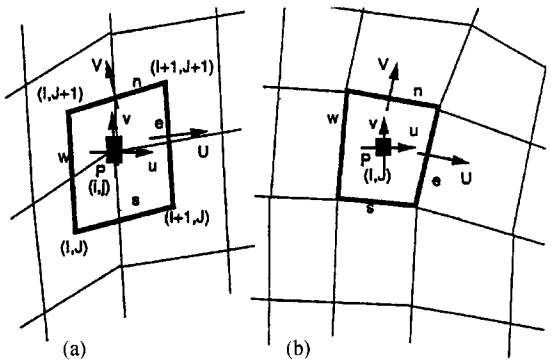

Fig. 1. Node-centered (left) and cell-centered arrangements.

whose dissipation coefficient is given by

$$d_{i+1/2,j,k} = \alpha_{i+1/2,j,k}[\varepsilon^{(2)}_{i+1/2,j,k}\delta_x \boldsymbol{W}_{i,j,k} - \varepsilon^{(4)}_{i+1/2,j,k}\delta_{xxx}\boldsymbol{W}_{i-1,j,k}]. \tag{10}$$

The dissipation flux $d_{i+1/2,j,k}$ is of third order in smooth regions. However, in regions of high pressure variations, the dissipation is of first order and the scheme behaves as a first order upwind scheme. The difference operators of first and third order are δ_x and δ_{xxx}, respectively,

$$\delta_x \boldsymbol{W}_{i,j} = \boldsymbol{W}_{i+1,j} - \boldsymbol{W}_{i,j}, \tag{11}$$

$$\delta_{xxx}\boldsymbol{W}_{i,j} = \boldsymbol{W}_{i+2,j} - 3\boldsymbol{W}_{i+1,j} + 3\boldsymbol{W}_{i,j} - \boldsymbol{W}_{i-1,j}, \tag{12}$$

and α is the scaling factor, which is written for the i direction according to (Blazek, 1994)

$$\alpha_{i+1/2,j,k} = \tfrac{1}{2}(\lambda^{i^*}_{i,j,k} + \lambda^{i^*}_{i+1,j,k}), \tag{13}$$

where the eigenvalues λ are scaled in each coordinate direction as

$$\lambda^{i^*}_{i,j,k} = \lambda^{i}_{i,j,k}.\phi^{i}_{i,j,k}, \tag{14}$$

considering the cell aspect ratio

$$\phi^{i}_{i,j,k} = 1 + \max\left[\left(\frac{\lambda^{j}_{i,j,k}}{\lambda^{i}_{i,j,k}}\right)^{w}, \left(\frac{\lambda^{k}_{i,j,k}}{\lambda^{i}_{i,j,k}}\right)^{w}\right]. \tag{15}$$

The coefficients adapted to the local pressure gradients $\varepsilon^{(2)}$ and $\varepsilon^{4)}$, needed to obtain the dissipation coefficient, are written as follows:

$$\varepsilon^{(2)}_{i+1/2,j,k} = k^{(2)}\max(\nu_{\max}), \tag{16}$$

$$\varepsilon^{(4)}_{i+1/2,j,k} = \max(0, k^{(4)} - \varepsilon^{(2)}_{i+1/2,j,k}), \tag{17}$$

$$v_{i,j,k} = \frac{p_{i+1,j,k} - 2p_{i,j,k} + p_{i-1,j,k}}{p_{i+1,j,k} + 2p_{i,j,k} + p_{i-1,j,k}}, \tag{18}$$

$$v_{\max} = (v_{i+2,j,k}, v_{i+1,j,k}, v_{i,j,k}, v_{i-1,j,k}), \tag{19}$$

is the 2nd order divided difference pressure sensor and $k^{(2)}$ and $k^{(4)}$ are

$$0.5 \leqslant k^{(2)} \leqslant 0.6, \tag{20}$$

$$\tfrac{1}{128} \leqslant k^{(4)} \leqslant \tfrac{1}{48}. \tag{21}$$

The spectral radius λ used to control the amount of artificial dissipation is defined based on the Mach number M for the i direction according to [2]

$$\lambda^i = \tfrac{1}{2}\left[u(1+M^2) + \sqrt{u^2(1-M^2)^2 + \beta^2 c^2}\right] \tag{22}$$

which reduces to $\lambda^i = u + c$ for $M \geqslant 1$ [6].

It is well known that for a central difference scheme, zero artificial viscosity creates numerical difficulties. Therefore β^2 is chosen according to

$$\beta^2 = \max(4M^2, \Phi), \tag{23}$$

where Φ is adopted as [3]

$$0.1 \leqslant \Phi \leqslant 0.6. \tag{24}$$

4. Time-stepping

In order to obtain numerical solutions of high accuracy, the Runge–Kutta method is chosen [5]. This method is characterized by its low operation count. More than two stages are employed in order to extend the stability region. The following multistage scheme, which requires low computational storage is employed [6]

$$\boldsymbol{W}^{(0)}_{i,j,k} = \boldsymbol{W}^{n}_{i,j,k}, \tag{25}$$

$$\boldsymbol{W}^{r}_{i,j,k} = \boldsymbol{W}^{(0)}_{i,j,k} - \frac{\alpha_r \Delta t \boldsymbol{R}^{(r-1)}_{i,j,k}}{V_{i,j,k}}, \tag{26}$$

$$\boldsymbol{W}^{n+1}_{i,j,k} = \boldsymbol{W}^{(r)}_{i,j,k}, \tag{27}$$

where

$$\boldsymbol{R}^{r}_{i,j,k} = \boldsymbol{Q}^{r}_{i,j,k} - \boldsymbol{D}^{(r)}_{i,j,k}, \tag{28}$$

with $r = 0, 1, 2, \ldots, m = 5$, and the coefficients $\alpha_1 = 1/4$, $\alpha_2 = 1/6$, $\alpha_3 = 3/8$, $\alpha_4 = 1/2$, $\alpha_5 = 1$.

5. Boundary conditions

The numerical treatment of boundary conditions in the physical domain is one of the major problems in solving the Euler equations. Inappropriate conditions can substantially degrade the accuracy

of convergence of the computed solution. Numerical conditions imposed at the outer boundary should assure that the outgoing waves are not reflected back into the flow field, specially when solving subsonic or mixed flows (regions).

In order to establish an efficient numerical implementation of the boundary conditions the computational domain is surrounded by dummy cells. Using a body fitted coordinate system the boundary coinciding with a coordinate line is approximated by a straight lines in the finite volume approximation. On a solid boundary the physical condition of no normal flow can be imposed.

6. Numerical results

In the following, numerical results for a launch vehicle are presented and compared with available data. First computations were performed for launch vehicle for supersonic Mach 3.75. Supersonic flows are high speed flows that appear for reentry launch vehicles or high speed aircrafts. These flows are characterized by strong shocks, contact discontinuities and regions of highly expanded flows.

Computations were performed for typical(old) launch vehicle geometry, as shown in Fig. 2. Fig. 3 displays the bidimensional grid for SVL (Satellite Vehicle Launcher) nose, which consists of 62×26 cells. The corresponding pressure coefficient is presented in Fig. 4 and is compared with experimental data [8].

Fig. 5 displays the computational grid employed for three-dimensional geometry, which consists of $140 \times 28 \times 7$ cells. It is a complex grid that covers 1/8 of the circumference of the SVL geometry.

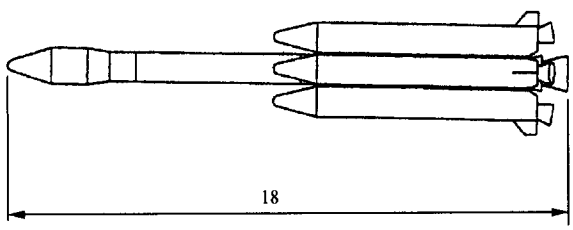

Fig. 2. A SVL (Satellite Vehicle Launcher) geometry.

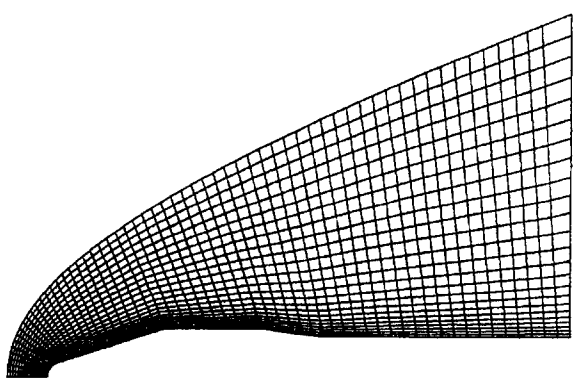

Fig. 3. Grid for SVL, 62×26 cells.

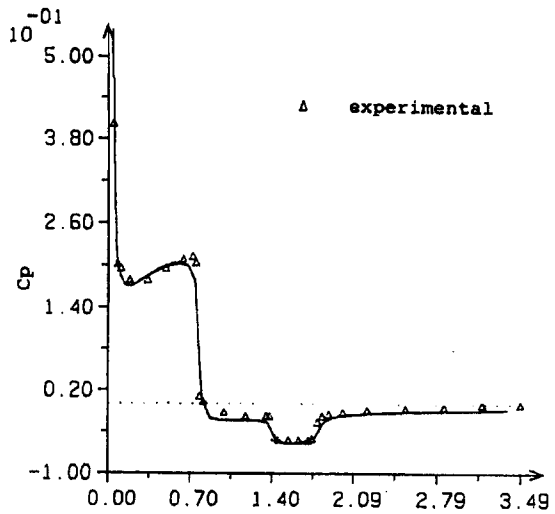

Fig. 4. Comparison of pressure coefficient for SVL nose, Mach = 3.75.

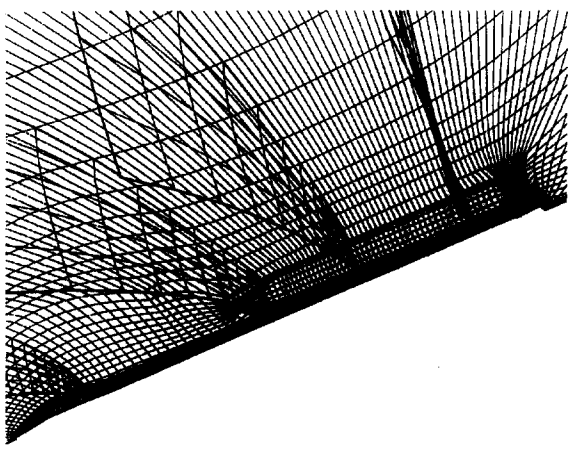

Fig. 5. Grid for SVL, 140 × 26 × 7 cells.

A complete vehicle is obtained reproducing and rotating conveniently this grid. Pressure contours, as presented in Fig. 6, indicate the need for grid refinement among the boosters and between the booster and the central body.

Comparison of the pressure coefficient distribution over the frontal part of the vehicle indicates good agreement with the experimental solution. The comparison of the pressure coefficient for the whole vehicle is currently under way. Finally, a color pressure map for the launch vehicle is presented, as shown in Fig. 7.

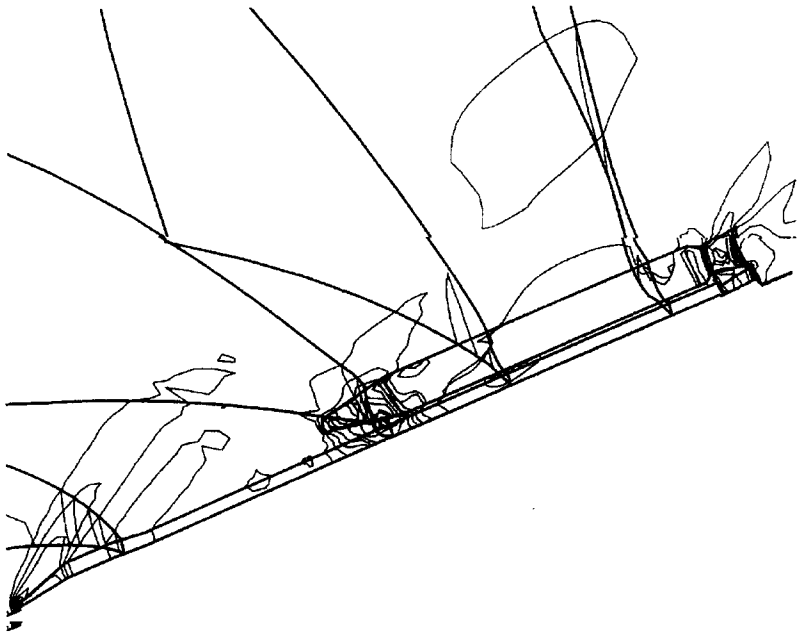

Fig. 6. Pressure contours for SVL, Mach = 2.0.

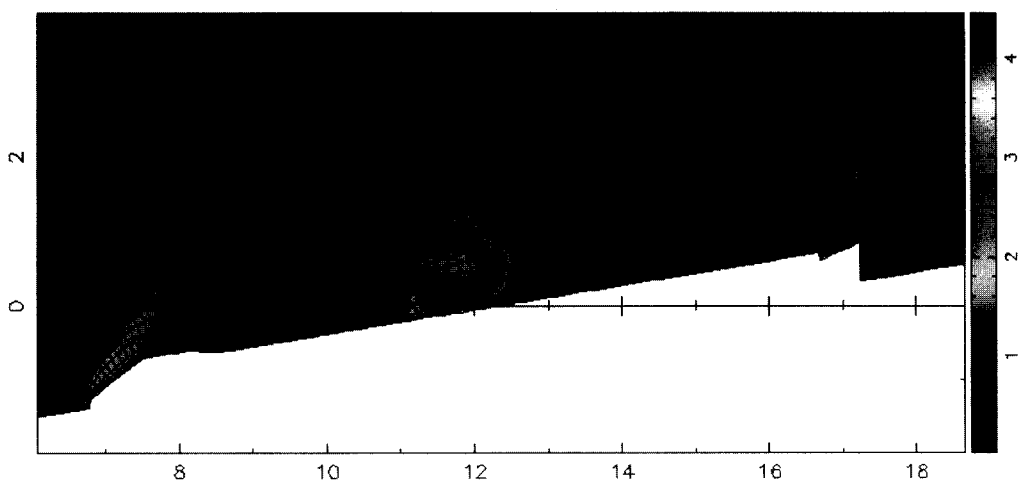

Fig. 7. Color pressure map for 3D launch vehicle, Mach = 2.0.

7. Conclusions

Tests have shown that the numerical method based on finite volume spatial discretization, the Runge–Kutta time-stepping scheme and on preconditioning, can be used to solve compressible fluid flows around complex geometries. Accuracy of the code has been tested in computing subsonic, transonic and supersonic flows around airfoils and wings [1,3].

Special care has been taken in the treatment of the influence of limit coefficients used to evaluate the time-step and the artificial dissipation. Numerical tests indicate that the dissipation coefficient can be chosen between 1/48 and 1/128 without modifying the results.

It is the author's opinion that the comparison between the experimental and numerical solutions is encouraging. However, a lot of work must still be done in order to obtain and compare the pressure coefficient for the complete vehicle geometry.

Acknowledgements

The author would like to thank Dr. Norbert Kroll and Dr. Jiri Blazek for sharing their experiences concerning the Euler version of CEVCATS and their many insights into Computational Fluid Dynamics, when he visited DLR – Institute of Design Aerodynamics in Braunschweig (Germany).

References

[1] J. Blazek, Verfahren zur Beschleunigung der Lösung der Euler- und Navier–Stokes Gleichungen bei Stationaren Über- und Hyperschallströmungen, Ph.D. Thesis, University of Braunschweig, 1994.

[2] Y.H. Choi, C.L. Merkle, The application of preconditioning in viscous flows, J. Comput. Phys. 105, (1993) 207–223.

[3] A.L. De Bortoli, Solution of incompressible flows using compressible flow solvers, DLR IB 129/94-18, Braunschweig, Germany, 1994, pp. 1–86.

[4] A.L. De Bortoli, Convergence acceleration applied to solve compressible and incompressible fluid flows, J. Brazilian Soc. Mech. Sci., XIX, (3), (1997) 357–370.

[5] A. Jameson, W. Schmidt, E. Turkel, Numerical solution of the Euler equations by finite volume methods using Runge–Kutta time-stepping schemes, AIAA Paper 1981, 81–1259.

[6] N. Kroll, R.K. Jain, Solution of two-dimensional Euler equations – experience with a finite volume code, Forschungsbericht, DFVLR-FB 87-41, Braunschweig, Germany. 1987.

[7] N. Kroll, C.-C. Rossow, Foundations of numerical methods for the solution of Euler equations, Prepared for Lecture F 6.03 of CCG, Braunschweig, Germany, 1989.

[8] C.R. Maliska, A.F.C. Silva, Technical Reports to IAE/CTA – Parts I–IX (1987–1991), Essai du Lanceur Brasilien AU 1/15, December 1988.

[9] R. Radespiel, A cell-vertex multigrid method for the Navier–Stokes equations, NASA Technical Memorandum 101557, 1989.